RSC Advances

ROYAL SOCIETY OF CHEMISTRY

www.rsc.org/advances

ARTICLE TYPE www. rsc.org/xxxxxx | XXXXXXXX

Electron induced chemistry of Thiophene

Minaxi Vinodkumar,*[a] Hardik Desai,[b‡] and P C Vinodkumar[b]

Received Xth XXXXXXXXXX 20XX, Accepted Xth XXXXXXXXX 20XX
First published on the web Xth XXXXXXXXXX 200X
DOI: 10.1039/b000000x

Comprehensive theoretical study of electron scattering with thiophene over a wide impact energy range is reported in this article. Total, elastic, differential and momentum transfer cross sections were computed at low energy using ab initio R-matrix method through QUANTEMOL-N. The R-matrix calculations were carried out using Complete Active Space - Configuration Integration (CAS-CI) method employing Static Exchange (SE) and Static Exchange plus Polarization (SEP) models. Beyond ionization threshold, from intermediate to high energy the calculations were carried out using Spherical Complex Optical Potential (SCOP) formalism. There is a smooth crossover of the two formalisms at the overlap energy and hence we are able to predict the cross sections over a wide energy range. Apart from the scattering cross section calculations the other focus was to obtain resonances which are important features at low energy. We observed three prominent structures in the total cross section (TCS) curve. The first peak at 2.5 eV corresponds to formation of $\sigma*$ resonance which is attributed to Feshbach resonance, in good agreement with earlier predicted experimental and theoretical values at 2.65 eV and 2.82 eV respectively. The second peak observed at 4.77 eV corresponds to the shape resonance that resembles to earlier predicted experimental values of 5 eV and 5.1 eV, which is attributed to ring rupture. The third peak at 8.06 eV is attributed to core excited shape resonance. There is lone previous theoretical data for total cross section by da Costa et. al. [R. F. da Costa, M. T. do N. Varella, M. Lima, and M.Bettega, 2013, *J. Chem. Phys.* **138**, 194306] from 0 to 6 eV and no other theoretical or experimental work is reported at low energy to the best of our knowledge. Hence the present work is important to fill the void of the scattering data as the earlier work is fragmentary. The differential, momentum transfer and excitation cross sections beyond 6 eV are reported for the first time.

1 This is the section heading style

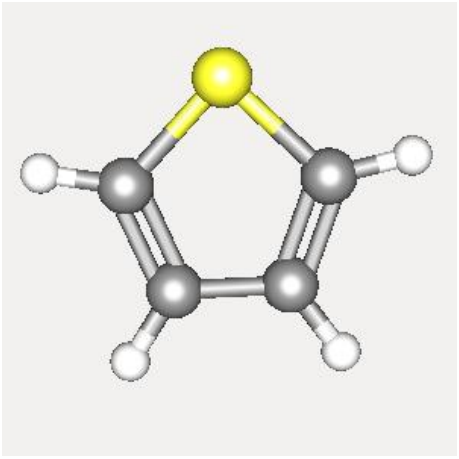

Fig. 1 (color online): Schematic diagram of Thiophene molecule

Thiophene (Fig. 1) is one of the most important and largely studied heterocyclic aromatic compounds[1–3], yet it remains a focal point of on-going research owing to central role it plays in the challenges facing modern science and technology. Specifically the materials that include thiophene units, such as thiophene polymers and oligomers, possess various important properties[4–6], which make them promising as photochromatic molecular switches[7–9], organic semiconductors[10,11], solar cells[12,13], light-emitting diodes and field-effect transistors[14–16]. For many of these applications, understanding the fundamental electronic structure, spectroscopy, photophysics and scattering data of thiophene is of primary importance. Hence considerable efforts are constantly being made to gain further knowledge in these fields. Apart from these industrial importance, the low energy electron impact studies for bio-molecules and related systems have gained prominence after the pioneering work reported by Boudaffa et al.[17]. Now it is well accepted that bond cleavages in DNA produced by impact of slow secondary electrons occur through the formation of transient negative ion formation (anions). It is worth mentioning that the formation of such metastable states (transient negative ion formation) is a very efficient way to release energy to the nuclear degrees of freedom especially through vibrational channel. As a result, the process may

[a] *V P & R P T P Science College, Vallabh Vidyanagar - 388 120, India; E-mail: minaxivinod@yahoo.co.in*
[b] *Department of Physics, Sardar Patel University, Vallabh Vidyanagar - 388120, India; E-mail:hardikdesai.phy@gmail.com; E-mail:p.c.vinodkumar@gmail.com*

eventually give rise to one or more separated fragments which is also known as a dissociative electron attachment (DEA). Therefore, it becomes imperative that the understanding and the characterization of resonances represent important steps towards a deeper insight into the damage induced to DNA through DEA mechanisms[18]. Looking to the importance of such studies of thiophene it is surprising that not much work is carried out on electron impact studies. Todate, the low energy electron impact studies is carried out recently by da Costa et al.[20], where they reported electron impact integral, momentum transfer and differential cross sections for thiophene molecules using Schwinger multichannel method for very low impact energies from 0.5 eV to 6 eV. Mozejko et. al.[19] reported integral elastic cross sections from 40 eV to 3000 eV and ionization cross sections from threshold to 3000 eV using Binary Encounter Bethe (BEB) method. Apart from these Modelli and Burrow[21] reported electron transmission spectra for Thiophene. Very recently Holland et. al.[22] resolved photoabsorption spectrum between 5 and 12.5 eV and Hedhili et al.[23] reported measurements for electron impact on multilayer thiophene condensed on a polycrystalline platinum substrate. Wehlitz and Hartman[24] studied double ionization of thiophene using monochromatized synchrotron radiation over a wide range of photon energies in combination with the ion time of flight technique. Zhang et. al.[25] measured the binding energy spectrum and momentum distributions of the valence orbitals of thiophene using electron momentum spectroscopy. Haberkern et. al.[26] measured high-resolution electron-energy-loss spectra of thiophene in the range of the low-lying singlet-triplet excitations. Muftakhov et. al.[44] studied the dissociative attachment of electrons to thiophene in gas phase in the energy range 0 - 12 eV. Looking to the literature survey it is quiet evident that electron impact scattering studies are very scarce and in absence of any experimental data and fragmentary theoretical data, present study will be quite meaningful and important. In the present work we study electronic excitation cross sections,differential cross sections, momentum transfer cross sections and total cross sections for e-C_4H_4S scattering.

Electron-molecule collision cross sections from very low energy up to threshold play an important role in determining electron transport properties and electron energy distribution of a swarm of electrons drifting through various gases. They also play significant role in modeling low temperature plasmas. In addition to the practical interest, electron scattering data are of fundamental theoretical importance towards the understanding of various electron assisted molecular chemistry[27]. The electron bombardment on a molecule may result into the formation of positive and negative ions. The latter may be produced by resonance attachment, dissociative resonance capture and ion-pair formation.These mechanisms provide us vast understanding about various chemical changes that will take place with the target at different electron energies. The resonance processes usually occur in the 0-10 eV energy region and the ion-pair processes at energies above 10 eV.

This paper is organised as follows, in Section 2 we describe first the target model and then describe the salient features of theoretical methodologies employed for low energy as well as high energy calculations. Section III is devoted to results and discussions of the results obtained and finally we end up with conclusions of the present study.

2 THEORETICAL METHODOLOGY

Considerable progress is made in the experimental and theoretical study of electron-molecule collision processes in the past decades. By utilizing better electron spectrometers and adopting position-sensitive detectors, experimentalists are capable of producing accurate cross-sectional data on electron collisions with larger molecules and even explore free radical species. However, given the vast number of molecular systems and the requirement for an ever-increasing amount of data, the experimental community are unable to meet the demands of the myriad of data users. In this respect one must look to theory to provide much of the required electron-scattering data. On the theoretical front, with the advent of high-performing computers and the development of very accurate theories, computation of reliable cross-section data is now possible at least for smaller targets. These theoretical methods are computationally taxing and consume longer computing time. Thus, there is a demand for more generic and faster calculations to provide reliable data to the user community.

For the low energy (0.01 eV to about 20 eV), we employed the ab initio calculations using QUANTEMOL − N[28] which utilizes UK molecular R-matrix code[29], while the SCOP method is employed for calculating total (elastic plus inelastic) cross sections beyond ionization threshold up to 5 keV[30]. Salient features of these two formalisms are briefly discussed in the following subsections. Before going to the details of the theoretical methods we also discuss the target model employed for the present system.

2.1 TARGET MODEL

The accuracy of scattering data depends on the accuracy of the target wave function, hence, it is advisable to have an appropriate target model. For many-electron targets like C_4H_4S, the relative energy between the N-target electrons and

the N+1 − target plus scattering electron becomes important since neither the target nor the scattering wave functions have the energies close to the exact value for the given system. This requires careful choice of the configurations in terms of a complete active space (CAS) and the valence configuration interaction (CI) representation of the target system[28]. It is realized by characterizing the low lying electronic states of the target and by generating a suitable set of orbitals. The molecular orbitals are generated by performing a self-consistent field (SCF) calculation of the ground state of the molecule ($X1A_1$). Since the SCF procedure is inadequate to provide a good representation of the target states, we improve the energies of these states by invoking the variational method of configuration interaction (CI) in which we take linear combination of configuration state functions (CSFs) of a particular overall symmetry. This lowers the energies and the correlation introduced provides a better description of the charge cloud and the energies. For all the states included here, we employ CI wave function to represent the target states.

The Hartree-Fock electronic configuration for the ground state of C_4H_4S at its equilibrium geometry in C_{2v} point group symmetry is $1a_1^2$, $1b_2^2$, $2a_1^2$,$3a_1^2$, $2b_2^2$, $4a_1^2$, $3b_2^2$, $5a_1^2$, $1b_1^2$, $6a_1^2$, $4b_2^2$, $7a_1^2$, $8a_1^2$, $5b_2^2$, $9a_1^2$, $6b_2^2$, $10a_1^2$, $7b_2^2$, $2b_1^2$, $11a_1^2$, $3b_1^2$, $1a_2^2$. Out of total 44 electrons, 36 electrons are frozen in $1a_1$, $2a_1$, $3a_1$, $4a_1$, $5a_1$, $6a_1$, $7a_1$, $8a_1$, $9a_1$, $10a_1$, $11a_1$, $1b_1$, $2b_1$, $1b_2$, $2b_2$, $3b_2$, $4b_2$, $5b_2$, $6b_2$, $7b_2$ molecular orbitals and 8 electrons are kept free to move in active space of $3b_1$, $4b_1$, $8b_2$, $1a_2$ molecular orbitals. We employed 6-311G* Gaussian type orbitals (GTO) and Double Zeta plus Polarization (DZP) basis sets.

The target wave functions are computed using the complete active space configuration integration (CAS−CI) method. They are subsequently improved using a pseudo-natural orbital calculation. The Born correction for this polar molecule is employed to account for higher partial waves, $l > 4$. In the static-exchange-polarization (SEP) model, the ground state of the molecule is perturbed by single and double excitations of the electrons, thus leading to the inclusion of polarization effects. The SEP model augments the Static - exchange (SE) model by including polarization effects. Thus polarization effects are accounted by including closed channels in a CI expansion of the wave function of the entire scattering system. These electronic and angular momentum channels altogether generated 864 configuration state functions (CSFs) and 138 channels in the calculation.

The Quantemol-N modules GAUSPROP and DENPROP[31] are employed to construct the transition density matrix from the target eigenvectors obtained from Configuration Integration (CI) expansion and generates the target properties. The multipole transition moments obtained are then used to solve the outer region coupled equations and the dipole polarizability α_0. These are computed using second-order perturbation theory and the property integrals are evaluated by GUASPROP[31]. Our self-consistent field (SCF) calculations yielded target parameters such as the ground state energy, the first electronic excitation energy, rotational constant, dipole moment and ionization energy which are listed in Table 1.

The self-consistent field calculations yielded the ground state energy of -551.35 Hartree and -551.34 Hartree using 6-311G* and DZP basis sets, which are in very good agreement with -551.37 Hartree reported by Zhang et. al.[25]. We report 10 electronic excitation states below ionization threshold of the target for thiophene with the first electronic excitation energy obtained at 4.51 eV using 6-311G* and at 4.46 eV using DZP basis set as listed in Table 1. The present first excitation energy is close to 4.7 eV reported by Palmer et. al.[32] and slightly lower compared to 5.64 eV reported by Holland et. al.[22]. The present rotational constant of 0.2683 cm^{-1} is in perfect agreement with the theoretical value of 0.2683 cm^{-1} reported in CCCBDB (Computational Chemistry Comparison and Benchmark DataBase)[33]. The present computed dipole moment is 0.79 D obtained using 6-311G* and 0.68 D obtained using DZP basis sets are close to measured value of 0.64 D reported by Zhang et. al[25] and slightly higher compared to 0.55 D reported by CRC[37] and Ogata et. al[35] and 0.53 D reported by Pozdeev et. al.[36]. It can be easily seen that dipole moment is very sensitive to the basis set chosen. DZP basis set gives better target property calculations for thiophene as compared to 6311G* basis set as evident from the Table 1. The present calculated ionization threshold is 8.91 eV and 8.93 eV using 6311G* and DZP basis sets as against 8.87 eV and 8.86 eV reported by Palmer et. al.[32] and reported in CCCBDB[33] respectively. Table 2 shows vertical excitation energies for thiophene obtained using 6311G* and

Table 1 Target properties obtained for the C_4H_4S molecule using 6-311G* and DZP basis sets

Target property (Unit)	Present		Other
	6-311G*	DZP	Th./Exp.
Ground State Energy (Hartree)	-551.35	-551.34	-551.37[25]
First Excitation Energy (eV)	4.51	4.46	5.78[22]
			5.64[22]
			3.8[32]
Rotational Constant (cm^{-1})	0.2683	0.2683	0.2683[33]
Dipole Moment (Debye)	0.79	0.64	0.55[34]
			0.64[25]
			0.55[35]
			0.53[36]
Ionization Potential (eV)	8.91	8.93	8.87[32]
			8.86[33]

DZP basis sets.

Table 2 Vertical excitation energies for Thiophene below ionization threshold for 6-311G* and DZP basis sets

6-311G*		DZP	
State	**Energy (eV)**	**State**	**Energy (eV)**
$1A_1$	0.00	$1A_1$	0.00
$3B_2$	4.51	$3B_2$	4.46
$3A_1$	5.71	$3A_1$	5.52
$3B_1$	7.41	$1A_1$	7.24
$1B_1$	7.59	$3A_1$	7.54
$3A_2$	7.68	$3B_1$	7.57
$1A_2$	7.89	$1B_2$	7.67
$1B_2$	7.98	$3A_2$	7.68
$1A_1$	8.28	$1B_1$	7.88
$3A_2$	8.44	$1A_2$	7.98
$1A_2$	8.52	$3B_2$	8.01

2.2 Low energy formalism (0.01 $\sim$ 20 eV)

The low energy calculations use close coupling method in which the total wave function of the system (e + molecule) is represented as superposition of the ground state and all excited states wave functions of the target. The most popular methodologies employed for low-energy electron collision calculations are the Kohn variational method[38,39], the Schwinger multichannel method[40,41], and the R-matrix method[29] which make use of close coupling (CC) method. Out of three methods, the R matrix is the most widely used method. The basic idea behind the R-matrix method[29] is to split the configuration space describing the scattered electron and target into an inner region, which is a sphere of radius 'a' about the target center of mass, and an outer region. The boundary between these two regions is defined by R-matrix radius. This radius is chosen large enough so that, in the external region, only known long-range forces are effective and anti-symmetrization effects such as exchange and electron - electron correlation can be neglected. In fact in the internal region where the scattered electron has penetrated the charge distribution of the target, the interaction is strong. In the inner region full electron-molecule problem is solved using Quantum Chemistry codes. The inner region is usually chosen to have a radius of around 10 au and the outer region is extended to about 100 au. The choice of this value depends on the stability of results obtained in the inner region and outer region calculations. We describe the scattering within the fixed-nuclei (FN) approximation that neglects any dynamics involving the nuclear motion (rotational as well as vibrational), whereas the bound electrons are taken to be in the ground electronic state of the target at its optimized nuclear geometry. This is an effect of the extent of electronic charge density distribution around the center of mass of the target. In the present study we considered 13 au for inner R-matrix radius.

In the inner region the total wave function for the system is written as,

$$\Psi_k^{N+1} = A\sum_I \Psi_I^N(x_1,...,x_N)\sum_j \zeta_j(x_{N+1})a_{Ijk} + \sum_m \chi_m(x_1,...,x_{N+1})b_{mk} \quad (1)$$

where A is the antisymmetrization operator, x_N is the spatial and spin coordinate of the nth electron, ζ_j is a continuum orbital spin-coupled with the scattering electron and a_{Ijk} and b_{mk} are variational coefficients determined in the calculation. The summations in the first term runs over the target states used in the close-coupled expansion. The summation in the second term runs over configurations χ_m, where all electrons are placed in target molecular orbitals. The number of these configurations varies considerably with the model employed. With the wave function given by Eqn. 1, a static exchange calculation has a single Hartree-Fock target state in the first sum. The second term runs over the minimal number of configurations usually 3 or fewer, required to relax orthogonality constraints between the target molecular orbitals and the functions used to represent the configuration. Our fully close-coupled system uses the lowest number of target states represented by a CI expansion in the first term and over a hundred configurations in the second. These configurations allow for both orthogonality relaxation and short-range polarization effects.

The target and the continuum orbitals are represented by Gaussian Type Orbitals and the molecular integrals are generated by the appropriate Molecular Package. The R-matrix will provide the link between the inner region and outer region. For this purpose the inner region is propagated to the outer region potential until its solutions match with the asymptotic functions given by the Gailitis expansion[29]. Thus by generating the wave functions, using Eq. 1, their eigenvalues are determined. These coupled single centre equations describing the scattering in the outer region are integrated to identify the K - matrix elements. The K - matrix is a symmetric matrix whose dimensions are the number of channels. All the observables are basically deduced from it and further it is used to deduce T matrix using the relation:

$$T = \frac{2iK}{1-iK} \quad (2)$$

The T - matrices are in turn used to obtain various total cross sections. The K $-$ matrix is diagonalized to obtain the eigenphase sum. The eigenphase sum is further used to obtain the position and width of the resonance by fitting them

to the Breit Wigner profile[42] using the program RESON[42]. General diagrams for the 'QUANTEMOL - N', UK molecular R- matrix codes[43] for the target calculations, Inner region calculations and outer region calculations are presented wide Fig. 2, Fig. 3 and Fig. 4 respectively.

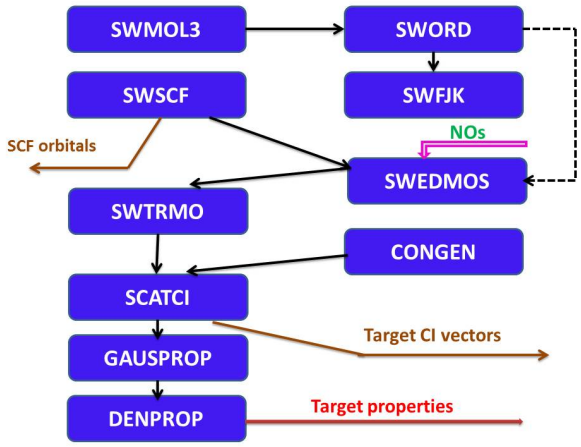

Fig. 2 (color online): Structure of a target calculation in the polyatomic UK Molecular R-matrix codes

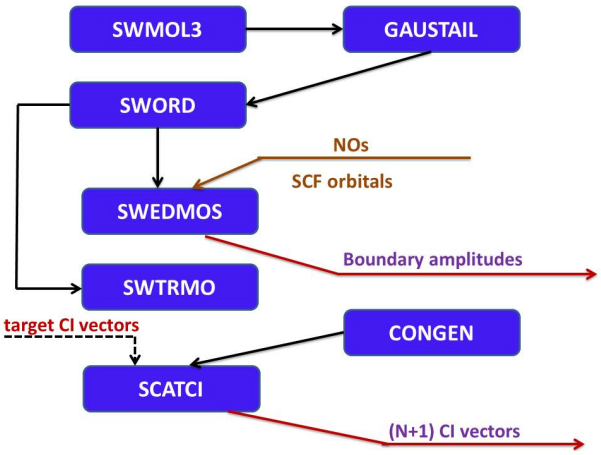

Fig. 3 (color online): Structure of the inner region calculation for the polyatomic UK Molecular R-matrix codes

Fig. 2 shows the steps taken to generate target wave functions and associated properties as a prelude to a full scattering run[31]. The first three modules, SWMOL3, SWORD and SWFJK perform the necessary integral evaluation. SWTRMO convert integrals in atomic orbitals to integrals over molecular orbitals which are used in the (CI) calculation. SWEDMOS makes orbital set orthonormal by Schmidt orthogonalization. The configuration generation for the Hamiltonian Matrix

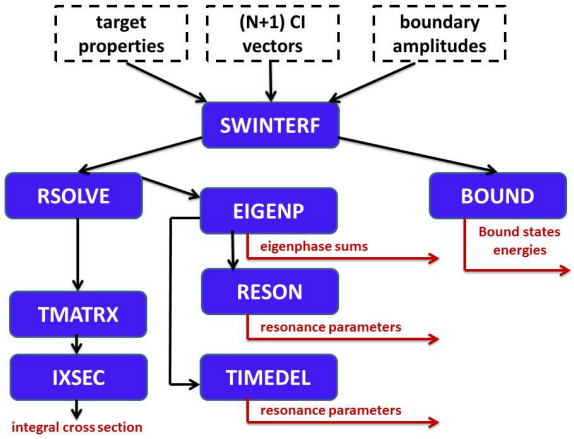

Fig. 4 (color online): The main modules used in the outer region of the polyatomic UK Molecular R-matrix codes

is done by CONGEN. SCATCI is the workhorse of the inner region calculation that constructs Hamiltonian matrix and diagonalizes it. Modules GAUSPROP and DENPROP calculates target properties. It should be noted that molecular R-matrix with pseudo states (RMPS) calculations involve running the target section twice. Fig. 3 shows modules involved in inner region calculations. The integral over atomic orbitals are again computed using SWMOL3 and those involving continuum orbital are adjusted for finite dimension of R-matrix radius using GAUSTAIL. Thus target properties, (N+1) CI vectors and boundary amplitudes computed using inner region calculation goes as input for outer region calculation.

Unlike the inner regions codes the outer region is run as a single program. Fig. 4 shows important modules used for scattering calculations. SWINTERF acts as the boundary between the inner region and outer region codes. It reads in the target properties, boundary amplitudes, R-matrix pole positions and associated eigenvectors from inner region. From these it constructs a list of asymptotic channels necessary to construct the R-matrix. RSOLVE is the main workhorse of the outer region code. The output from RSOLVE is a set of K-matrices and TMATRX is used to turn K-matrices to T-matrices which in turn through IXSEC gives integral cross sections. Module EIGENP diagonalizes the K-matrix to give the eigenphase sum which is analyzed for resonances by RESON. TIMEDEL fits these resonances and provides position and width of resonances. POLYDCS[45] calculates differential and momentum transfer cross sections.

Differential Cross section (DCS) study is very important as it provides large information about the interaction processes.

Indeed, the evaluation of DCS is stringent test for any scattering theory as it is sensitive to effects which are averaged out in integral cross sections. The DCS for polyatomic molecule is represented by:

$$\frac{d\sigma}{d\Omega} = \sum_L A_L P_L(cos\theta) \tag{3}$$

where, P_L represents the Legendre polynomial of order L. The details about A_L are already discussed by Gianturco and Jain[46]. For a polar molecule this expansion over L converges slowly due to long range nature of dipole potential. To overcome this problem we use the closure formula given by:

$$\frac{d\sigma}{d\Omega} = \frac{d\sigma^B}{d\Omega} + \sum_L (A_L - A_L^B) P_L cos\theta \tag{4}$$

Here the subscript, B denotes the fact that the relevant term is calculated under Born Approximation with an electron point dipole interaction. It is clear that convergence of the series is faster as the contribution arising from Born term is subtracted as seen in Eqn. 4. The quantity $\frac{d\sigma^B}{d\Omega}$ for any initial rotor state is given by the sum over all final rotor states as

$$\frac{d\sigma^B}{d\Omega} = \sum_{J'\tau'} \frac{d\sigma^B}{d\Omega}(J\tau \rightarrow J'\tau') \tag{5}$$

The calculated dipole moment (D) and rotational constants (A=0.2683 cm^{-1}, B=0.1804 cm^{-1}, C=0.1079 cm^{-1}) for $(CH)_4S$ are used in the calculation of elastic DCS (J=0 $\rightarrow$ J'=0) and rotationally inelastic (J=0 $\rightarrow$ J' = 1, 2, 3, 4 and 5) DCSs at different collision energies.

In fact the MTCS is obtained by integrating the differential cross sections (DCS) with a weight factor (1-cosθ).

$$\sigma_m = 2\pi \int \frac{d\sigma}{d\Omega}(1 - cos\theta) d\theta \tag{6}$$

2.3 Higher energy formalism (Threshold to 5 keV)

The R-matrix calculations cannot be extended beyond 20 eV even with the latest modern computers due the complexities involved in the scattering calculations. Hence, the scattering calculations above the ionization threshold are studied using the SCOP formalism[30,47]. In this formalism, the electron-molecule system is represented by a complex optical potential comprising of real and imaginary parts as,

$$V_{opt}(r, E_i) = V_R(r) + iV_I(r, E_i) \tag{7}$$

such that,

$$V_R(r, E_i) = V_{st}(r) + V_{ex}(r, E_i) + V_p(r, E_i) \tag{8}$$

where, E_i is the incident energy. Eq. 8 corresponds to various real potentials to account for the electron target interaction namely, static, exchange and the polarization potentials respectively. These potentials are obtained employing the target geometry, molecular charge density of the target, the ionization potential and polarizability as inputs. The molecular charge density may be derived from the atomic charge density by expanding it from the center of mass of the system. The molecular charge density so obtained is renormalized to account for the total no. of electrons present. The atomic charge densities and static potentials (V_{st}) are formulated from the parameterized Hartree-Fock wave functions given by Cox and Bonham[48].

The parameter free Hara's free electron gas exchange model[49] is used to account for any exchange between the incoming electron and one of the target electron through the exchange potential (V_{ex}). The polarization potential (V_p) arises from the transient redistribution of target charge cloud due to incoming electron which gives rise to dipole and quadrupole moments. This potential is formulated from the parameter free model of correlation-polarization potential given by Zhang et al.[50]. Here, various multipole non-adiabatic corrections are incorporated in the intermediate region which will approach the correct asymptotic form at large r smoothly. The target parameters like ionization potential (IP) and dipole polarizability (α_0) of the target used here are the best available from the literature[51].

The imaginary part in V_{opt}, called the absorption potential V_{abs} accounts for the total loss of flux scattered into the allowed inelastic channels namely discrete electronic excitations channels or excitations leading to continuum states i.e. ionization channels. The expression used here are vibrationally and rotationally elastic. This is due to the fact that the non-spherical terms do not contribute much to the total potential at the present high energy range.

The well-known quasi-free model of Staszeweska et al.[52] is employed for the absorption part, given by,

$$V_{abs}(r, E_i) = -\rho(r)\sqrt{\frac{T_{loc}}{2}}\left(\frac{8\pi}{10k_F^3 E_i}\right) \theta(p^2 - k_F^2 - 2\Delta)(A_1 + A_2 + A_3) \tag{9}$$

Where T_{loc} is the local kinetic energy of the incident electron which is given by,

$$T_{loc} = E_i - (V_{st} + V_{ex} + V_p) \tag{10}$$

Here $p^2 = 2E_i$ and $k_F = [3\pi^2\rho(r)]^{\frac{1}{3}}$ is the Fermi wave vector and A_1, A_2 and A_3 are dynamic functions that depend differently on $\theta(x)$, I, Δ and E_i. Here, 'I' is the ionization threshold

of the target, $\theta(x)$ is the Heaviside unit step-function and Δ is an energy parameter below which V_{abs} = 0. Hence, Δ is the principal factor which decides the values of total inelastic cross section, since below this value ionization or excitation is not allowed. This is one of the main characteristics of Staszewska model[52]. This has been modified by us by considering Δ as a slowly varying function of E_i around I. Such an approximation is meaningful since Δ fixed at I would not allow excitation at energies $E_i \leq I$. However, if Δ is much less than the ionization threshold, then V_{abs} becomes unexpectedly high near the peak position. The amendment introduced is to give a reasonable minimum value 0.8I to Δ[53] and also to express the parameter as a function of E_i around I, i.e.,

$$\Delta(E_i) = 0.8I + \beta(E_i - I) \quad (11)$$

Here the parameter β is obtained by requiring that Δ = I (eV) at $E_i = E_p$, the value of incident energy at which present Q_{inel} reaches its peak. E_p can be found by calculating Q_{inel} by keeping $\Delta = I$. Beyond E_p, Δ is kept constant and is equal to I. The expression given in Eqn. 11 is meaningful as Δ fixed at the ionization potential would not allow any inelastic channel to open below I. Also, if it is much less than I, then V_{abs} becomes significantly high close to the peak position of Q_{inel}. This has been elaborately discussed in our earlier paper by Vinodkumar et. al.[53]

The complex potential thus formulated is used to solve the Schrödinger equation numerically through partial wave analysis. This calculation will produce complex phase shifts for each partial wave which carries the signature of interaction of the incoming projectile with the target. Phase shifts are the key ingredients for all scattering calculations. At low energies only a few phase shifts (5-6 for absorption and 100 for polarization at ionization threshold) are significant, but as the incident energy increases more phase shifts (around 40 for absorption and 100 for polarization) are needed for convergence. The phase shifts δ_l thus obtained are employed to find the relevant cross sections, total elastic (Q_{el}) and the total inelastic cross sections (Q_{inel}) using the scattering matrix $S_l(k) = exp(2i\delta_l)$[54]. Then the total scattering cross section (TCS), Q_T is obtained by adding these two cross sections[54].

3 RESULTS AND DISCUSSION

The present work reports total cross sections for e - C_4H_4S scattering. We have employed the ab initio R matrix code below the ionization threshold of the target. In this energy range the total cross section is sum of total elastic and total electronic excitation cross sections. Above it, we have computed the total cross section as the sum of total elastic and total inelastic cross section using the SCOP formalism. With amalgamation of these two formalisms we are able to predict the total cross sections over wide energy range[55–58]. The numerical results of total cross sections for C_4H_4S are reported from 0.01 eV to 5000 eV as listed in Table 3 and are also plotted graphically.

Table 3 Total Cross Section (TCS) for the e - C_4H_4S Scattering (Energies (E) are in eV and TCS' are in $Å^2$)

E	R-matrix*	E	R-matrix*	E	SCOP†	E	SCOP†
0.01	626.48	4.89	50.70	19	28.22	700	5.29
0.25	46.82	5	50.56	20	27.32	800	4.78
0.5	39.48	6	44.18	30	26.11	900	4.37
0.75	37.61	7	40.36	40	26.51	1000	4.03
1	36.89	8	39.36	50	24.80	2000	2.65
1.5	36.38	9	37.87	60	22.70	3000	2.25
2	36.88	10	36.42	70	20.91	4000	1.84
2.45	54.49	11	35.69	80	19.45	5000	1.44
2.47	54.80	12	34.97	90	18.24	–	–
2.5	54.57	13	33.13	100	17.22	–	–
3	40.08	14	31.71	200	12.72	–	–
3.5	39.65	15	31.26	300	9.59	–	–
4	42.13	16	31.38	400	7.88	–	–
4.5	47.78	17	30.65	500	6.75	–	–
4.75	50.24	18	29.51	600	5.92	–	–

∗TCS calculated using R-matrix formalism
†TCS calculated using SCOP formalism

It is important to study eigenphase diagrams as they provide the positions of resonances which are important features of collision chemistry in the low energy regime. Resonances are a common characteristic of electron molecule scattering at low impact energies and lead to distinctive structure in pure vibrational excitation cross sections[59]. Resonances occur when the incident electron is temporarily captured by the target to form a negative ion (an anion) which subsequently decays either by autodetachment (often leaving the target vibrationally/electronically excited) or by dissociating the molecule to produce a net product anion (a process known as Dissociative Electron Attachment (DEA). In the last few decades of development of negative ion mass spectrometry of resonant dissociative electron attachment considerable progress has been achieved in understanding the fragmentation process. Presently a recursive procedure for detecting and performing Breit Wigner fits to the eigen phase diagram is done through program RESON[42]. This program generates new energy points and marks those points where the numerically computed values of second derivative changes sign from positive to negative. Finer grids are constructed about each of these points which are used as inputs for Briet Wigner fit[42] and two most important parameters (Position and width) related to resonances are obtained.

Table 4 gives the positions and widths of resonances obtained in the present case using R-matrix calculations.

Table 4 Position and width of resonance states for C_4H_4S

	Present			Others
State	Basis state	Position	Width	Position
$2B_1$	DZP	2.51	0.33	2.82[20]
$2A_2$	DZP	4.35	1.28	5.3[23]
	-	-		5.35[44]
	-	-		5.48[44]
$2A_2$	6-311G*	7.77	0.01	8.5[44]
$2A_1$	6-311G*	10.70	0.56	9.5[23]
	-	-		10.2[44]
$2B_1$	DZP	11.36	0.13	11[23]
$2A_2$	DZP	11.97	0.84	-
$2A_2$	DZP	13.21	0.16	-
$2A_2$	DZP	14.40	0.06	-
$2A_2$	DZP	15.17	0.05	16[23]
$2B_1$	6-311G*	17.60	0.46	-
$2B_2$	6-311G*	17.83	0.46	-
$2A_2$	DZP	17.90	0.57	-
$2A_1$	DZP	18.51	1.24	-
$2A_2$	6-311G*	18.51	0.33	-
$2B_2$	DZP	18.69	1.10	-
$2B_2$	DZP	18.73	0.84	-
$2A_1$	DZP	19.48	1.62	-

Hedhill et. al.[23] and Muftakhov et. al.[44] have performed detailed study on DEA. Muftakhov et. al.[44] detected formation of C_2H^-, S^-, SH^-, $C_3H_2^-$, $SC_2H_2^-$, SC_2H^-, $C_2H_3^-$, C_4H^-, $SC_4H_2^-$ and $SC_4H_3^-$ anions in the energy range 0 to 12 eV. The resonances were observed at 3.5 eV, 5.3 eV, 6.4 eV, 8.5 eV, 8.9 eV and 10.2 eV by Muftakhov et. al.[44]. The resonances detected by Hedhill et. al.[23] were at 3.8 eV, 4.7 eV, 5 eV, 6.5 eV, 12.1 eV, 12.7 eV, 13.3 eV, 13.9 eV and 14.3 eV. The present position and width of the resonances calculated using Briet Wigner Profile are listed in Table 4. We observed the resonances at 2.51 eV, 4.35 eV, 7.77 eV, 10.7 eV, 11.36 eV, 11.97 eV, 13.21 eV, 14.40 eV, 15.17 eV, 17.6 eV, 17.83 eV, 17.90 eV, 18.51 eV, 18.69 eV, 18.73 eV and 19.48 eV. Muftakhov et. al.[44] suggested that resonance observed at 5.3 eV involved excitation of the molecule into the lowest singlet state and electron capture into a diffuse molecular orbital of a quasi-Rydberg state. We observed this resonance at 4.77 eV which is close to 5.3 eV reported by Muftakhov et. al.[44] and at 5 eV reported by Hedhill et. al.[23]. Ion yields seen above 6.5 eV were assigned to core-exited resonances in which the incident electron and a second electron, promoted from a inner orbital, reside in quasi-Rydberg states. Resonance like structures are readily apparent in the yield functions of C_2H^- and C_2HS^- at 11 eV and 16 eV. The resonances above 16 eV may be attributed due to dissociative desorption process. The resonances reported in Table 4 are responsible for fragmentation of C_4H_4S into various anions C_2H^-, S^-, SH^-, $C_3H_2^-$, $SC_2H_2^-$, SC_2H^-, $C_2H_3^-$, C_4H^-, $SC_4H_2^-$ and $SC_4H_3^-$ at different energies.

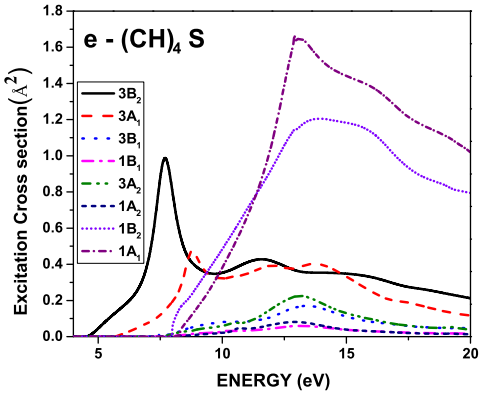

Fig. 5 (color online): e - C_4H_4S Excitation cross sections from the ground state (X $1A_1$) to the $3B_2$ - Solid line, $3A_1$ - Dash line, $3B_1$ - Dot line, $1B_1$ - Dash dot, $3A_2$ - Dash dot dot, $1A_2$ - Short dash, $1B_2$ - Short dot, $1A_1$ - Short dash dot

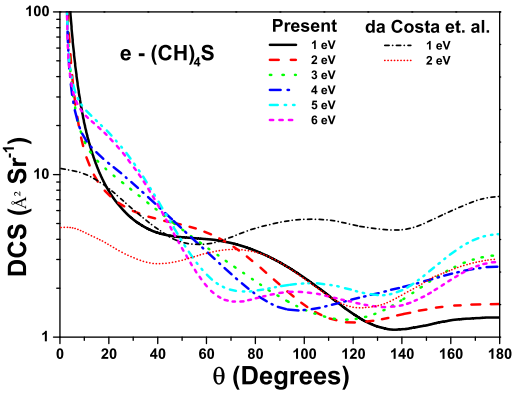

Fig. 6 (color online): Rotationally resolved Differential Cross Sections (DCS) for incident energies of 1 eV to 6 eV; Present (Thick lines): Solid line - 1 eV, Dash line - 2 eV, Dot line - 3 eV, Dash dot line - 4 eV, Dash dot dot line - 5 eV, Short dash line - 6 eV; da Costa et. al.[20] (Thin lines): Short dash dot line - 1 eV, Short dot line - 2 eV

Fig. 6 shows sum of our rotationally resolved differential cross sections summed over all transitions (J=0 to J'= 0 to 5) for incident energies 1 eV, 2 eV, 3 eV, 4 eV, 5 eV, 6 eV,

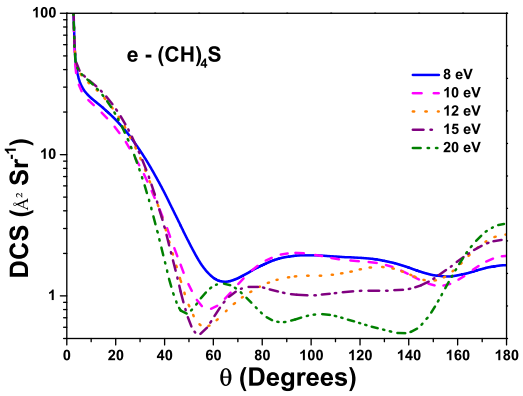

Fig. 7 (color online): Rotationally resolved Differential Cross Sections (DCS) for incident energies of 8 eV, 10 eV, 12 eV, 15 eV and 20 eV; Present : Solid - 8 eV, Dash - 10 eV, Dot - 12 eV, Dash dot - 15 eV,Dash dot dot - 20 eV

while Fig. 7 shows the same for incident energies 8 eV 10 eV, 12 eV, 15 eV and 20 eV. da Costa et. al.[20] have reported differential cross sections for 1 eV, 2 eV, 3 eV, 4 eV, 5 eV, 6 eV. The scattering is dominated by elastic component 0 $\rightarrow$ 0 and dipole component 0 $\rightarrow$ 1. The elastic component shows two minima centred at 40° and 108° in 1 eV curve, which indicates the dominance of a p-wave in the interference pattern arising due to various partial wave amplitudes. The results of da Costa et. al.[20] are qualitatively in agreement and the position of minima is also comparable. For 2 eV curve the position of minima occur around 40° and 120° in agreement with the results of da Costa et. al.[20]. For 3 eV curve there is a single minima observed at around 129° both in present case as well in results of da Costa et. al.[20]. At 4 eV the minima is around 98° for both the present and da Costa et. al.[20] data. At 5 eV and 6 eV the present DCS results show two minima while the results of da Costa et. al.[20] show single minima. This discrepancy may be attributed to the difference in the treatment of polarization effect and in partial wave cut off for the Born corrections adopted in the two calculations[60]. We have compared present DCS results with that of da Costa et. al.[20] for 1 eV to 6 eV but for brevity of figure we have compared our results for 1 eV and 2 eV with that of da Costa et. al.[20]. As the energy increases the convergence with respect to J is rapid. The divergence at the forward angle is confirmed as being due to dipole allowed transitions 0$\rightarrow$1 dominating the scattering. The differential cross sections decrease as the incident energy increases. The sharp enhancement in the forward direction is a result of the strong long-range dipole component of the interaction potential. In absence of any comparisons either theoretical or experimental for 8 eV, 10 eV, 12 eV, 15 eV and 20 eV, we plotted all DCS curves in the same figure (Fig. 7).

The Momentum Transfer Cross Sections (MTCS) indicate the importance of the backward scattering and are important quantity that forms the input to solve the Boltzmann equation for the calculation of electron distribution function for swarm of electrons drifting through a molecular gas. In contrast to the divergent behavior of DCS in the forward direction, the MTCS does not diverge due to the multiplicative factor (1 - cosθ). A further test of the quality of our DCS is shown by the momentum transfer cross section (MTCS) in figure 8 from energies 0.01 eV to 20 eV. The MTCS cross sections are computed for SEP and SE models. In thiophene there is long lived $\sigma*$ shape resonance which is seen as a peak in MTCS curve at 2.79 eV which is in excellent agreement with the same resonance predicted at 2.78 eV by da Costa et. al[20]. We also predict a strong peak at 4.86 eV which is not observed in the MTCS curve of da Costa et. al.[20]. The various peaks or structures observed in MTCS correspond to various resonance processes. Present MTCS curves for both SE and SEP approximations are in good agreement with the results of da Costa et. al.[20]. No other theoretical or experimental comparisons are reported for thiophene.

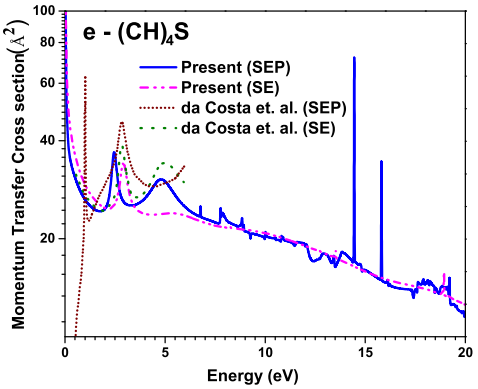

Fig. 8 (color online): e - C_4H_4S Momentum Transfer Cross Section (MTCS); Present : SEP - Solid line, SE - Dash dot dot line; da costa et. al.[20]: SEP - Short dot line, SE - Dot line

Due to the presence of long range dipole interaction, the total cross section at low energy is diverging in the fixed nucleii approximation due to singularity in the differential cross section in the forward direction. It is well known that the cross sections of dipole dominated processes only converge slowly with partial waves. To obtain converged cross sections, the effect of rotation must be included along

with a large number of partial waves. The higher partial waves ($l \geq 4$) are included using a Born correction as given in the work of Chu and Dalgarno[61]. This is done by adjusting the T-matrices using the CC cross sections generated by the code POLYDCS[45]. In this procedure our low l T-matrices are added to analytic dipole Born T- matrices using the adiabetic nuclear rotation (ANR)[62–64]. The Born contribution for partial waves higher than $l = 4$ to the elastic cross section at energies below 0.5 eV is quite large as seen from Fig. 10.

For brevity, the total cross sections for $e - C_4H_4S$ scattering results are plotted in two figures. The target model employed for the present calculations is CAS (c) = 3, Number of states per symmetry (n) = 3 and R-matrix radius (r) = 13, abbreviated as c3n3r13. In figure 9, we have compared low energy (0 to 20 eV) total cross sections data for $e - C_4H_4S$ scattering using 6-311G* and DZP basis sets with lone theoretical data of da Costa et. al[20]. They have done calculations for impact energies 0 to 6 eV only. The present calculations for total cross section at low energy are carried out using both SE and SEP models. We observe three prominent structures for SEP approximation employing DZP basis set and two prominent structures using 6311G* basis set. They are at 2.5 eV, 4.77 eV and 8.06 eV with peak values of total cross sections as 56.87 $Å^2$, 51.91 $Å^2$ and 38.11 $Å^2$ respectively. The first peak corresponds to formation of $\sigma*$ resonance which can be attributed to Feshbach resonance as predicted by da costa et. al.[20] and Muftakhov et. al.[44]. The second peak observed at 4.77 eV corresponds to the resonance which was suggested to involve excitation of the molecule into the lowest singlet state and electron capture into a diffuse molecular orbital of a quasi-Rydberg state by Muftakhov et. al.[44]. They observed this peak at 5.3 eV which is very close to present value of 4.77 eV . The third peak at 8.06 eV is attributed to core excited shape resonance. The present SE approximation yields three structures at 3.0 eV, 6.45 eV and 12.49 eV with cross sections values of 54.93 $Å^2$, 40.92 $Å^2$ and 37.68 $Å^2$ respectively. It is quiet evident that SEP approximation gives more refined calculations and the resonance peaks shifts to lower energy. The elastic cross sections of da Costa et. al.[20] are qualitatively in good agreement with present results with their second peak 2.52 eV of 45.66 $Å^2$ very close to our peak at 2.50 eV of 56.87 $Å^2$ of the $\sigma*$ shape resonance. The lower peak at 0.53 eV of 59.24 $Å^2$ predicted by da Costa et. al.[20] is not observed in our calculations. There are no other theoretical or experimental results reported to the best of our knowledge.

Finally in Fig.10 we report the total cross section for $e - C_4H_4S$ scattering over a wide range of impact energies starting from 0.01 eV to 5000 eV. We are able to report the total cross sections over such a wide range due to smooth cross over of the data obtained through two methodologies, viz. low energy data using R-matrix through QUANTEMOL-N and intermediate to high energy data through SCOP formalism. We find a smooth transition of the present data using 6 311G* as well as DZP basis set with the SCOP data at 17.2 eV and 19.9 eV respectively. The only high energy data for total cross section is reported by Mozejko et. al.[19] who have employed additivity rule for their calculations. The total cross sections reported by Mozejko et. al.[19] are higher compared to present data as expected and the discrepancy decreases with increase in the energy. No structure is observed in the data of Mozejko et. al.[19] as they used additivity rule which do not include any molecular properties in their calculation. No other theoretical or experimental data are reported so far.

Beyond 40 eV no prominent structures are found in total cross section curve. We would like to point out that in the present intermediate to high-energy region, the static term dominates over the exchange and polarisation contributions. In the SCOP approach we obtain information on the absorption cross sections due to all allowed inelastic channels. At intermediate energies (from threshold to up to about 200 eV) the electronic excitations diminish and the inelastic channel for electron-molecule collisions correspond to the direct and dissociative ionization dominates. As expected, the V_{abs} has no dominant long-range effect and it penetrates towards the inner shells with an increase in energy. We also note that the electronic and vibrational excitations are very small in this energy range to make any sizeable contributions to the total cross sections. Beyond 200 eV, the total cross sections follow Born Bethe decline. At intermediate to high energies (20 eV - 5000 eV) the cross sections are of relevance in applied areas such as plasma deposition, etching processes in semiconductor industry and electrostatic precipitators for the processing of atmospheric pollutants. The present target molecule, thiophene is of special interest as it is an important molecule in aeromatics which is a fascinating and rapidly evolving field, in which the various cross sectional data from low energy to high energies are employed in the kinetic modelling of reaction rates and understanding of the reaction mechanisms. There are no theoretical or experimental results available for this target beyond 6 eV to the best of our knowledge. So the present work may inspire more thoreticians/experimentalists to take up this task as thiophene is very important system from the point of view of its diverse applications as discussed in the introduction.

4 Conclusion

The elastic, differential, momentum transfer, excitation and total cross sections are reported for the first time for electron impact above 6 eV on C_4H_4S using the R-matrix method with

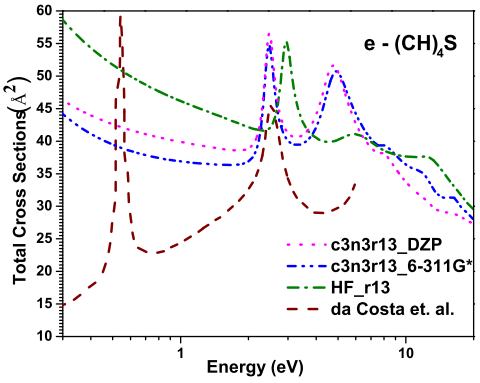

Fig. 9 (color online): e - C_4H_4S Total Scattering Cross Sections; c3n3r13 using: Dot lines - DZP basis set, Dash dot dot - 6-311G* basis set; Dash dot line - Present Hartree-Fock calculations; Dash line - da Costa et. al.[20]

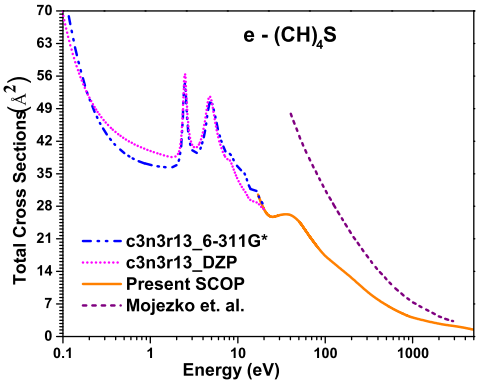

Fig. 10 (color online): e - C_4H_4S Total Scattering Cross Sections; c3n3r13 using: Dot lines - DZP basis set, Dash dot dot - 6-311G* basis set, Solid lines - Present SCOP, Short dash - Mozejko et. al.[19]

an adequate target representation. The total electron scattering cross sections for thiophene over a wide electron energy range is computed by adopting an amalgamation of two distinct theoretical methods vis a vis the ab-initio R- matrix (low energy - $0 \leq E_i \leq 20eV$) and the SCOP formalism for $E_i >$ threshold. The data computed using the two formalisms found to merge smoothly at 17.2 eV for results obtained using 6331G* and at 19.9 eV using DZP basis set. The present data for total cross sections at low energy is in good agreement with the previous data reported by da Costa et. al.[20]. This composite formalism is therefore able to produce a robust set of total cross section data when used in tandem (Table 3).

Further, the computed target properties such as the ground state energy, first electronic excitation energy, dipole moment, ionization potential and rotational constant match very well with the earlier predicted theoretical and experimental results as evident from Table 1. In Table 2 we have reported ten electronic excitation energy states for thiophene using DZP and 6-311G* basis sets. We observed formation of σ^* shape resonance at 2.51 eV which is close to experimentally predicted $\sigma*$ resonance by Modelli and Burrow at 2.65 eV and theoretically predicted resonance at 2.82 eV by da Costa et. al.[20]. The second peak observed at 4.77 eV corresponds to the shape resonance which is very close to 5.1 eV reported by Muftaknov et. al[44] eV and this resonance is responsible for ring rupture which is reported to be at 5 eV by Hedhill et. al.[23]. The third peak at 8.06 eV is attributed to core excited shape resonance. The peaks at 11 eV and 16 eV are attributed to dissociate desorption process and leads to formation C_2H^- and C_2HS^-. The knowledge of the dissociation dynamics through these resonances for thiophene needs to be investigated further on the complex potential energy surfaces given by these resonant states. Such electron impact studies of thiophene have gained prominence due its manyfold applications as discussed in the introduction. Present work is important as there is paucity of electron impact studies on thiophene. Also the scattering data are important in developing models to estimate the radiation damage of the living cells due to radio therapy as secondary electrons produced during irradiation (e.g. in cancer therapy) can cause larger effects on the biomolecules.

5 Acknowledgement

Minaxi Vinodkumar acknowledges DAE-BRNS, Mumbai for the Major research project [37(3)/14/44/BRNS-2014] for financial support under which part of this work is carried out.

References

1 T. Eicher, S. Hauptmann and A. Speicher, The Chemistry of Heterocycles: Structures, Reactions, Syntheses, and Applications, Wiley-VCH, Weinheim, 2nd edn, (2003).
2 H. D. Hartough, The Chemistry of Heterocyclic Compounds, Wiley-Interscience, New York, (1952), vol. 3.
3 S. Gronowitz, The Chemistry of Heterocyclic Compounds,Wiley-Interscience, New York, (1992), vol. 44.
4 C. Taliani and W. Gebauer, in Handbook of Oligo- and Polythiophenes, ed. D. Fichou, Wiley-VCH, Weinheim, (1998), p. 361.
5 J. L. Bredas, J. Cornil, F. Meyers and D. Beljonne, in Handbook of conducting polymers, ed. T. A. Skotheim, R. L. Elsenbaumer and J. R. Reynolds, Marcel Dekker, New York, (1998), p. 1.
6 G. Barbarella, M. Melucci and G. Sotgiu, *Adv. Mater.*,2005,**17**, 1581.
7 G. Tsivgoulis and J. Lehn, *Adv. Mater.*,1997, **9**,39.

8 M. Irie, in Molecular Switches, ed. B. L. Feringa, Wiley-VCH, Weinheim, 2001, p. 37.
9 A. Staykov, J. Areephong, W. Browne, B. Feringa and K. Yoshizawa, *ACS Nano*, 2011, **5**,1165.
10 A. Facchetti, *Mater. Today*, 2007, **10**, 28.
11 C.Dimitrakopoulos and P.Malenfant, *Adv. Mater.*, 2002 **14**,99.
12 J. Chen and Y. Cao, *Acc. Chem. Res.*, 2009, **42**, 1709.
13 Y. Liang and L.Yu, *Polym. Rev.*, 2010, **454**,50.
14 A. Murphy and J. Frechet, *Chem. Rev.*, 2007, **107**, 1066.
15 T. Noda, H. Ogawa, N. Noma and Y. Shirota, *Adv. Mater.*, 1997, **9**, 720.
16 M. G. Harrison and R. H. Friend, in Electronic Materials: The Oligomer Approach, ed. K. Mullen and G. Wegner,Wiley-VCH, Weinheim 1998, p. 516.
17 B. Boudaiffa, P. Cloutier, D. Hunting, M. Huels, and L. Sanche, *Science*, 2000, **287**, 1658.
18 F. Martin, P. Burrow, Z. Cai, P. Cloutier, D. Hunting, and L. Sanche,*Phys. Rev. Lett.*, 2004, **93**, 068101.
19 P. Mozejkoa, E. Ptasinska-Denga, and Cz. Szmytkowski, *Eur. Phys. J. D* , 2012, **66: 44**.
20 R. F. da Costa, M. T. do N. Varella, M. Lima, and M.Bettega, *J. Chem. Phys.*,2013, **138**, 194306.
21 A. Modelli and P.Burrow, *J. Phys. Chem. A* 2004, **108**, 5721.
22 D. M. P. Holland, A. B. Trofimov,E. A. Seddon,E. V. Gromov,T. Korona, N. de Oliveira,L. E. Archer,D. Joyeux and L. Nahon, *Phys. Chem. Chem. Phys.*, 2014, **16(39)**, 21629.
23 M. N. Hedhili, P. Cloutier, A. D. Bass, T. E. Madey and L. Sanche, *J. chem. Phys.*, 2006, **125**, 094704 .
24 R. Wehlitz and T. Hartman, J. Phys.: Conf. Ser., 2014,**493** 012002.
25 S. Zhang, X. Ren, G. Su, C. Ning, H. Zhou, B. Li, G. Li and J. Deng, *Chem. Phys.*, 2006, **327**, 269.
26 H. Haberkern, K. Asmis, M. Allan and P. Swiderek, *Phys. Chem. Chem. Phys.*, 2003, **5**, 827.
27 I. Schneider, *Adv. At., Mol., Opt. Phys.*, 1994, **33**,183.
28 J. Tennyson, *J. Phys. B: At. Mol. Opt. Phys.*, 1996, **29**, 6185.
29 D. Bouchiha, J. D. Gorfinkiel, L. G. Caron, and L. Sanche, *J. Phys. B: At. Mol. Opt. Phys.*,2007, **40**, 1259.
30 A. Jain, and K.L. Baluja, *Phys. Rev. A*, 1992, **45**, 202.
31 J. Tennyson, *Physics Reports*, 2010, **491**, 29.
32 M.Palmer, I.Walker, and M.Guest, *Chem. Phys.*, 1999, **241**, 275.
33 Editor: Russell D. Johnson III , NIST Computational Chemistry Comparison and Benchmark Database, NIST Standard Reference Database number 101 Release 15b, August 2011, http://cccbdb.nist.gov
34 Nelson, R. D., Lide, D. R., and Maryott, A. A., Selected Values of Electric Dipole Moments for Molecules in the Gas Phase, Natl. Stand. Ref. Data Ser. - Nat. Bur. Stnds. 10, 1967.
35 T. Ogata and K. Kozima, *J. Mol. Spect.*, 1972, **42**, 38.
36 N. Pozdeev, L. Panikovskaya, L. Lisovaskaya and A. Khamamleev, *Chemical Abstracts*, 1968,**69**, 14593g .
37 D R Lide, CRC Handbook of Physics and Chemistry, 74th edn. (Chemical RubberCompany, Boca Raton, FL, 1993-94.
38 'Computational Methods for Electron Molecule Collisions',edited by W. M. Huo and F. A. Gianturco (Plenum, New York,1995).
39 B. I. Schneider and T. N. Rescigno, *Phys. Rev. A*, 1988, 37, 3749.
40 T. N. Resigno, C.W. McCurdy, A. E. Orel, and B. H. Lengsfield III, in Computational Methods for Electron Molecule Collisions, edited by W. M. Huo and F. Gianturco (Plenum, New York,1995), pp. 144
41 E Joucoski and M H F Bettega, *J. Phys. B: At. Mol. Opt. Phys.*, 2002, **35**, 783.
42 J. Tennyson and C. J. Nobel, *Comput. Phys. Commun.*, 1984, **33**, 421.
43 L.A. Morgan, J. Tennyson, C.J. Gillan, *Comput. Phys. Comm.*, 1988, **114**, 120.
44 M. Muftakhov et al., *J. Electron Spectrosc. Relat. Phenom.*, 1994, **69**, 165.
45 N. Sanna and F. A. Gianturco, *Comput. Phys. Commun.*,1998, **114**, 142.
46 F. A. Gianturco and A. Jain, *Phys. Rep.*, 1986, **143**, 347.
47 C. Limbachiya, M. Vinodkumar, and N. Mason, *Phys. Rev. A*, 2011, **83**, 042708.
48 H. L. Cox, and R. A. Bonham, *J. Chem. Phys.*, 1967, **47**, 2599.
49 S. Hara, *J. Phys. Soc. Japan*, 1967 **22**, 710.
50 X. Zhang, J. Sun, and Y. Liu, *J. Phys. B: At. Mol. Opt. Phys.*, 1992 **25**, 1893.
51 R. Lide, CRC Handbook of Chemistry and Physics (Boca Raton, FL: CRC Press) 2003.
52 G. Staszewska, D. W. Schewenke, D.Thirumalai, and D. G. Truhlar, *Phys. Rev. A*, 1983, **28**, 2740.
53 Minaxi Vinodkumar, Kirti Korot, P.C. Vinodkumar, *Int. J. of Mass Spectrometry*, 2011, **305**, 26.
54 C. J. Joachain, Quantum Collision Theory (Amsterdam: North-Holland) 1983.
55 M. Vinodkumar, C. Limbachiya, H. Desai, P.C. Vinodkumar, *Phys. Rew. A*, 2014 **89**, 062715.
56 M. Vinodkumar, C. Limbachiya, H. Desai, P.C. Vinodkumar, *J. Appl. Phys.*, 2014 **116**, 124702.
57 Minaxi Vinodkumar and Mayuri Barot, *J. Chem. Phys.*,, 2012 **137**, 074311.
58 Minaxi Vinodkumar, Chetan Limbachiya, Avani Barot, and Nigel Mason, *Phy. Rev. A*, 2012, **86**, 012706.
59 L. Andric, I. M. Cadez, R. I. Hall, and M. Zubeck, J. Phys. B: At. Mol. Opt. Phys., 1983, **16**, 1837.
60 M. A. Khakoo, J. Blumer, K. Keane, C. Campbell, H. Silva, M. C. A.Lopes, C. Winstead, V. McKoy, R. F. da Costa, L. G. Ferreira, M. A. P. Lima, and M. H. F. Bettega, *Phys. Rev. A*, 2008, **77**, 042705.
61 S. I. Chu and A. Dalgarno, *Phy. Rev. A*, 1974, **10**,788.
62 N. T. Padial, D. W. Norcross, and L. A. Collins, *J. Phys. B: At., Mol. Opt. Phys.*, 1981, **14**, 2901.
63 M. A. Morrison, *Adv. At. Mol. Phys.*, 1988, **24**, 51156.
64 D. Pastega, R. F. da Costa, Marco A. P. Lima, and Marcio, and H. F. Bettega, *Eur. Phys. J. D*,2014, **68**, 20.